

Probing magnetism in exfoliated VI_3 layers with magnetotransport

David Soler-Delgado,^{1,2} Feng-rui Yao,^{1,2} Dumitru Dumcenco,¹ Enrico Giannini,¹ Jiaruo Li,³
Connor A. Occhialini,³ Riccardo Comin,³ Nicolas Ubrig,^{1,2} and Alberto F. Morpurgo^{1,2,*}

¹*Department of Quantum Matter Physics, University of Geneva, 24 Quai Ernest Ansermet, CH-1211 Geneva, Switzerland*

²*Department of Applied Physics, University of Geneva, 24 Quai Ernest Ansermet, CH-1211 Geneva, Switzerland*

³*Department of Physics, Massachusetts Institute of Technology, Cambridge, Massachusetts 02139, USA*

(Dated: August 4, 2022)

We perform magnetotransport experiments on VI_3 multilayers, to investigate the relation between ferromagnetism in bulk and in exfoliated layers. The magnetoconductance measured on field-effect transistors and tunnel barriers shows that the Curie temperature of exfoliated multilayers is $T_C = 57$ K, larger than in bulk ($T_{C,\text{bulk}} = 50$ K). Below $T \approx 40$ K, we observe an unusual evolution of the tunneling magnetoconductance, analogous to the phenomenology observed in bulk. Comparing the magnetoconductance measured for fields applied in- or out-of-plane corroborates the analogy, allows us to determine that the orientation of the easy-axis in multilayers is similar to that in bulk, and suggests that the in-plane component of the magnetization points in different directions in different layers. Besides establishing that the magnetic state of bulk and multilayers are similar, our experiments illustrate the complementarity of magnetotransport and magneto-optical measurements to probe magnetism in 2D materials.

Atomically thin layers of many different materials have been produced by exfoliating bulk crystals of van der Waals bonded compounds [1, 2]. The crystalline structure of exfoliated layers is commonly assumed to be the same as that of the bulk parent crystals, and indeed experiments normally confirm this assumption. This is however not the case for many recently discovered atomically thin magnetic materials [3–9], whose structure in exfoliated form differs from that of the bulk, often resulting in drastically different magnetic properties [10–14]. Examples are provided by CrI_3 —whose multilayers are layered antiferromagnet with $T_C = 51$ K whereas bulk crystals are ferromagnets with $T_C = 60$ K [4, 15, 16]—and CrCl_3 —in which the interlayer exchange interaction in multilayers is approximately one order of magnitude larger than in the bulk [17].

VI_3 (see Fig. 1a) is an example of current interest, which exhibits conspicuous structural differences in bulk and exfoliated multilayers, accompanied by a magnetic response that appears to be strikingly different in the two cases. Bulk VI_3 crystals possess inversion symmetry and at $T_C = 50$ K undergo a transition into a ferromagnetic state, suggested to be of the Ising type [18, 19]. Recent experiments, however, showcase an unusual evolution of the magnetic properties below 40 K, which is indicative of a more complex magnetic state [18, 20–26]. Experimental observations include the splitting of diffraction peaks in neutron and X-Ray spectroscopy [20, 26]; the onset of a disproportionation between the (supposedly) structurally equivalent V atoms, detected by nuclear magnetic resonance [22]; a pronounced increase in the in-plane magnetic susceptibility found in magnetization measurements [18, 24, 25]

(see Fig. 1c); a 30 degree rotation around the direction normal to the layers of the six-fold symmetric in-plane easy axis, which occurs upon cooling between 40 and 30 K [21]. No magnetic state capable to explain all the observed phenomenology has been proposed.

The fewer experiments [19, 27, 28] reported on exfoliated layers indicate that the crystalline structure lacks inversion symmetry (for trilayers or thicker layers), and that a ferromagnetic state occurs below $T_C = 57$ K, a value significantly higher than the bulk T_C , in contrast to expectations [3, 4, 29]. Both scanning magnetometry and reflective magnetic circular-dichroism (RMCD) measurements [19, 28] exhibit a behavior consistent with Ising ferromagnetism at all temperatures, with no anomalies. It, therefore, appears that the behavior of multilayers differs—and is simpler—than that observed in the bulk, but it is unclear whether this conclusion is just a consequence of the few experimental techniques available that offer enough sensitivity to probe magnetism in thin layers.

Here, we investigate exfoliated VI_3 layers by means of magnetotransport experiments and show that—despite their different structural properties and larger critical temperature—their magnetic response is similar to the one observed in bulk crystals, and not consistent with that of an Ising ferromagnet [30]. Magnetotransport was measured using field-effect devices (Fig. 1d-e) and in devices in which VI_3 multilayers act as tunnel barriers (Fig. 1f-g). In both configurations, a ferromagnetic transition is observed at $T_C = 57$ K, consistently with earlier RMCD measurements [19]. Nevertheless, the tunneling magnetoconductance below T_C deviates qualitatively from that of an Ising ferromagnet and exhibits a behavior in line with that of bulk crystals. Specifically, below 40 K, the magnetoconductance measured in a magnetic field perpendicular to the planes becomes

* alberto.morpurgo@unige.ch

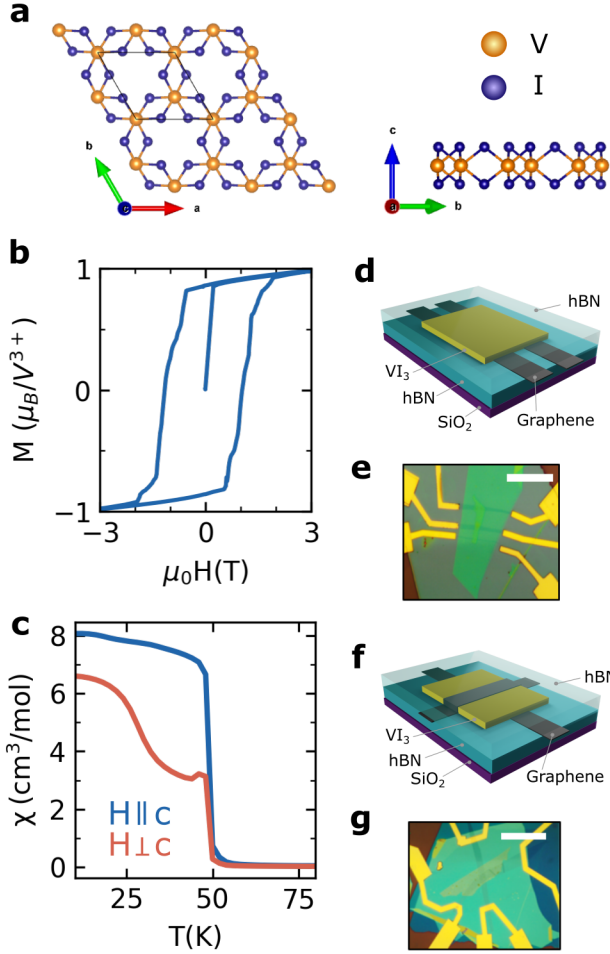


FIG. 1. (a) Top (left) and side (right) view of the crystal structure of a VI_3 monolayer. The purple and orange balls represent the iodine and vanadium atoms, respectively. (b) Magnetization, $M(H)$, of VI_3 bulk crystals measured at $T = 2$ K as function of magnetic field applied perpendicularly to the layers, showing hysteretic behavior. (c) Field-cooled susceptibility $\chi(T)$ ($\mu_0 H_{\perp} = 10$ mT) of our bulk VI_3 crystals, measured in a temperature range between $5 \text{ K} < T < 80 \text{ K}$. The blue and red curves denote measurement configurations where the magnetic field is applied parallel to the c -plane and ab -plane, respectively. Schematic representation (d) of a VI_3 transistor with graphene contacts and optical micrograph (e) of an actual device based on a 18 nm thick multilayer. The highly doped Silicon substrate covered by a 285 nm SiO_2 layer is used as gate (the scale bar is $10 \mu\text{m}$ long). Schematic representation (f) and optical micrograph (g) of a tunneling device, with graphene contacts on opposite sides of a 18 nm thick VI_3 multilayer (the scale bar is $10 \mu\text{m}$ long). All structures are encapsulated between hexagonal boron nitride (hBN) crystals to avoid degradation of VI_3 .

negative (whereas it is always positive in an established Ising ferromagnet such as CrBr_3 [30]), and the magnetoconductance in an in-plane field becomes pronouncedly hysteretic. By analyzing the magnetoconductance measured with the field applied in the two directions, we

determine that the easy axis in VI_3 multilayers forms an angle of approximately 30° with respect to the normal to the VI_3 planes. Such angle is close to –but smaller than– the that observed in bulk crystals. Besides showing that the magnetic state of exfoliated VI_3 multilayers and bulk crystals are similar, our results establish that the anomalous magnetic response originates from the in-plane component of the magnetization and illustrate the complementarity of magneto-optical and magneto-transport measurements to probe 2D magnetic materials.

The fabrication of VI_3 devices relies on micromechanical exfoliation of bulk crystals (characterized by magnetization and susceptibility measurements; see Fig. 1b and 1c) to obtain multilayers. The multilayers are processed to form field-effect transistors and tunnel barriers (see Fig. 1d-g), using conventional pick-up and transfer techniques based on polymeric stamps [31]. In practice, VI_3 multilayers are contacted with multilayer graphene strips and encapsulated in between exfoliated hBN layers (≈ 20 -50 nm thick) to avoid degradation (exfoliation and assembly of the structures are carried out in the controlled atmosphere of a glove box). We attach metal contacts to the graphene strips using conventional electron-beam lithography in combination with reactive ion etching, evaporation of a Cr/Au film, and lift-off. All structures are realized on highly doped Si substrates (acting as gates in transistor devices) covered with 285 nm SiO_2 . We have investigated two transistors and four tunnel junction devices that exhibit fully consistent behavior, and here we present representative data from a selected transistor and a selected tunnel junction (See the Supporting Information section S2 for data of additional devices).

We first discuss transport measurements performed on a VI_3 transistor (See Fig. 2a). Fig. 2b shows the transfer curves (*i.e.*, source-drain current I_{sd} as a function of gate voltage V_g), measured at $T = 90$ K, as V_{sd} is varied from 5 V to 1 V. The application of a positive gate voltage –corresponding to accumulating electrons at the surface of VI_3 – causes a large increase in current. Even at the largest positive gate voltage, however, the low-temperature resistance is extremely high and increases in a thermally activated fashion upon cooling (see Fig. 2c-d), indicating that the accumulated electrons are localized and that transport is mediated by hopping (the activation energy –approximately 50 meV at $V_g = +100$ V– corresponds to the distance in the energy of the localized electrons at the Fermi level and the conduction band). Under these conditions, it is unclear whether any magnetoconductance can be measured.

A magnetoconductance $\delta G(H_{\perp}, T) = (G(H_{\perp}, T) - G(0, T))/G(0, T)$ is nevertheless present, and exhibits a systematic evolution as a function of magnetic field applied perpendicularly to the layers, $\mu_0 H_{\perp}$, and temperature T (Fig. 2e). The magnetoconductance sets

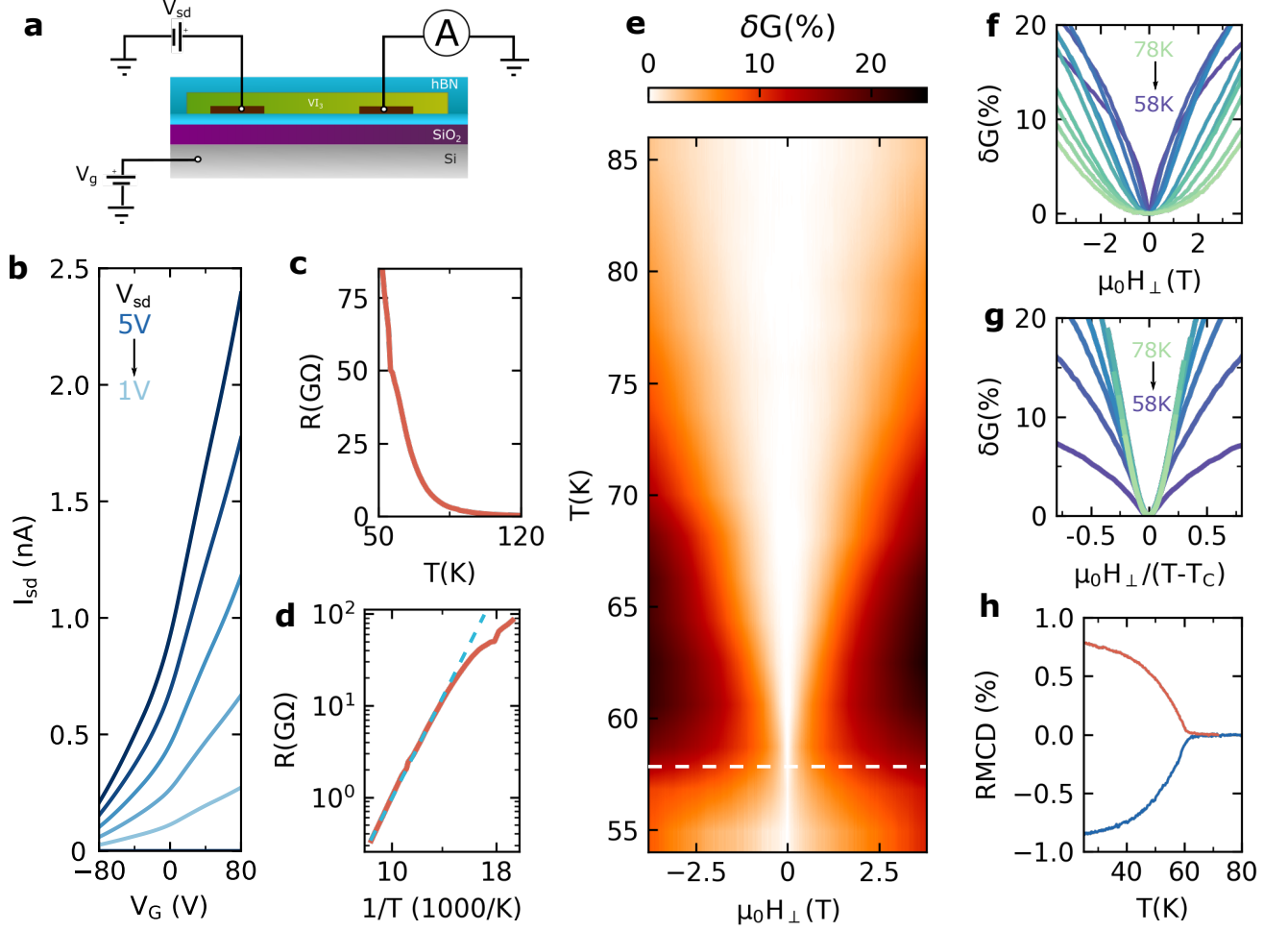


FIG. 2. (a) Schematic illustration of a field-effect transistor device used in the experiments. (b) Transfer curve (I_{sd} vs V_g) as the source-drain voltage is V_{sd} is varied from 5 V to 1 V in 1 V step. (c) Temperature dependence of the resistance, $R(T)$, of a VI_3 transistor measured with $V_{sd} = +8$ V and $V_g = +100$ V, exhibiting a pronounced increase upon cooling (d) logarithmic scale plot of $R(T)$ as a function of $1/T$. The linear dependence implies a thermally activated behavior with activation energy of $E_a \approx 50$ meV, as determined from a linear fit (blue dashed line). (e) False color plot of the in-plane magnetoconductance $\delta G(H_{\perp}, T) = (G(H_{\perp}, T) - G(0, T))/G(0, T)$ as a function of the magnetic field, $\mu_0 H_{\perp}$, applied along the c -axis and temperature T (the plot shows an interpolation of data measured at every 2 K as a function of $\mu_0 H_{\perp}$). The white dashed line indicates the ferromagnetic transition at $T_C = 57$ K. (f) Magnetoconductance δG for $T > T_C$, as T is varied from 78 K to 58 K, in 2 K steps. (g) Same data shown in (f) plotted as a function of $\mu_0 H_{\perp}/(T - T_C)$. When plotted in this way, all curves collapse on top of each other at small H_{\perp} . (h) Temperature dependence of the RMCD signal measured on a VI_3 tunnel barrier device based on a 10 nm thick VI_3 layer. The RMCD was measured in the region between the graphene tunnelling electrodes, while warming the sample up in the absence of a magnetic field, after having cooled down the device down to ~ 20 K in an applied perpendicular magnetic field of either +980 mT (red line) or -980 mT (blue line).

in at a lower magnetic field as the temperature T is lowered from 75 K to 58 K (see the horizontal dashed line), a manifestation of the critical regime in the paramagnetic state of VI_3 near the ferromagnetic transition. Specifically, for a ferromagnet the conductance is expected to increase as the VI_3 magnetization increases, *i.e.*, as the spins in the material orient themselves in the same direction. Since the magnetic susceptibility $\chi \propto 1/(T - T_C)$ diverges at T_C , a smaller value of $\mu_0 H_\perp$ is needed to generate the same magnetization as T approaches T_C , explaining why the magnetoconductance sets in at lower fields. Indeed, if we plot the magnetoconductance measured at different temperatures (Fig. 2f) as a function of $\mu_0 H_\perp/(T - T_C)$ (which in the linear regime is proportional to the magnetization) all curves overlap at small H_\perp (Fig. 2g). We conclude that—in the paramagnetic state—the magnetoconductance is a function of the magnetization and that the susceptibility tends to diverge as T approaches T_C . Optimizing the scaling of the magnetoconductance curves allows us to determine T_C to be 57 K (or more precisely between 56 K and 58 K; the precision of the method originates from the 2 K temperature interval with which data are taken).

In-plane transport measurements, therefore, confirm that exfoliated multilayers have a significantly higher T_C than the bulk. This value of the Curie temperature agrees well with the one determined in recent RMCD experiments [19], as well as in our own. Fig. 2h shows the temperature dependence of the circular-dichroism of the light reflected from a VI_3 exfoliated layer, measured at zero applied magnetic field, after having cooled down the multilayer to 20 K in either a +980 mT (red curve) or -980 mT (blue curve) applied field, to orient all magnetic domains and create a uniform magnetization. The signal originating from the magnetic circular dichroism indeed disappears close to 60 K.

For temperatures much lower than T_C the transistor resistance becomes higher than the sensitivity of our instruments, preventing the evolution of the magnetic state to be probed. Out-of-plane transport measurements on VI_3 tunnel barriers do not suffer from this limitation [16, 32–34] and in the remaining of this manuscript, we focus on these measurements to investigate magnetism in VI_3 exfoliated multilayers. Representative $I - V$ characteristics of a VI_3 multilayer tunnel barrier are shown in Fig. 3a. They exhibit a very pronounced non-linearity consistent with Fowler-Nordheim tunneling (see Fig. 3b): current flows when the applied bias tilts the bands in the VI_3 barriers and increases the tunneling transmission probability to a level that makes the tunneling current measurable, such that $\ln(I/V^2)$ depends linearly on $1/V$ at high bias [35].

Fig. 3c represents the tunneling magnetoconductance $\delta G(H_\perp, T) = (G(H_\perp, T) - G(0, T))/G(0, T)$ as a function of temperature, T , and magnetic field applied

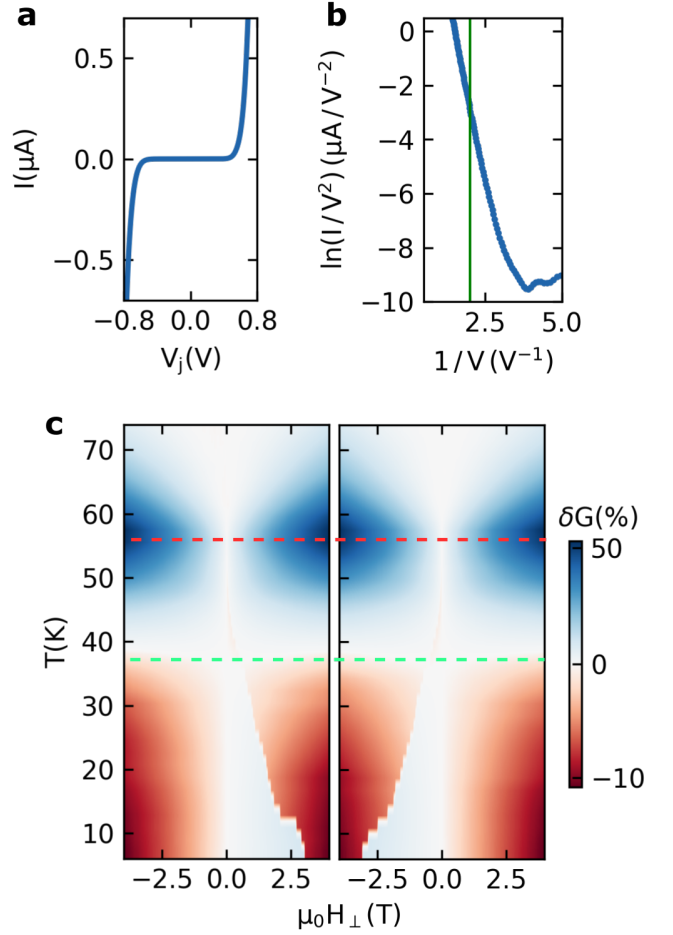


FIG. 3. (a) Current, I , across the tunnel barrier measured at $T = 2$ K as a function of voltage. (b) Similar to what is found in barriers made of different Chromium trihalides, at sufficiently large bias the current behaves as expected for Fowler-Nordheim tunneling, with $\ln(I/V^2)$ linearly proportional to $1/V$. The green solid line ($V = 0.5$ V) indicates the voltage at which the magnetoconductance data show in (c) (and in Fig. 4) were measured. (c) Color plot of tunneling magnetoconductance as a function of applied field $\mu_0 H_\perp$ and temperature T . Left and right panels represent the magnetoconductance measured while sweeping the field from -4 T to +4 T, or from +4 T to -4 T, respectively. The red dashed line in both panels indicates the Curie temperature T_C determined from the magnetoconductance data. The green dashed line in both panels denotes the temperature at which the magnetoconductance becomes negative ($T \approx 36$ K).

perpendicular to the layers, $\mu_0 H_\perp$, measured upon sweeping the field from either negative to positive (left) or from positive to negative (right) values. Because the $I - V$ curves are strongly non-linear, the absolute value of the conductance depends on applied bias, but the features observed in $\delta G(H_\perp, T)$ do not, *i.e.*, no qualitative aspect of the magnetoconductance on temperature and magnetic field dependence changes upon changing bias (see Supporting Information S3).

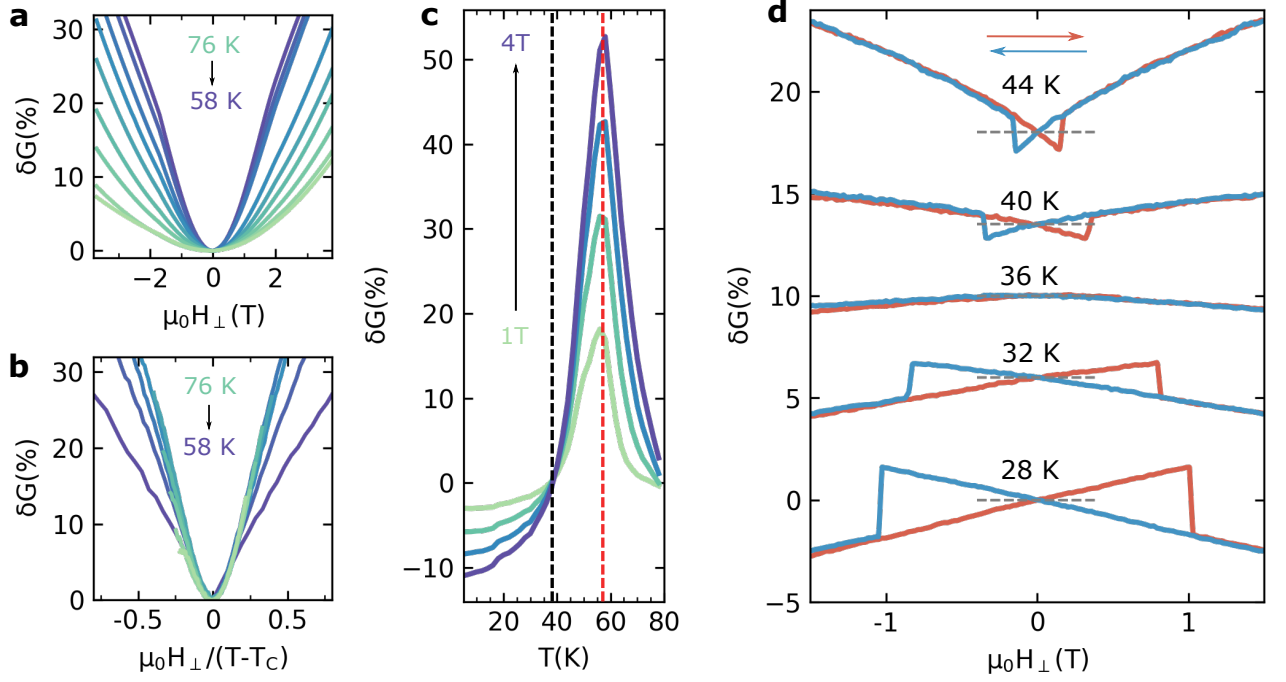


FIG. 4. (a) Magnetoconductance curves $\delta G(\mu_0 H_{\perp})$ for the temperature range between 76 K and 58 K, in 2 K steps. (b) same data as in panel (a) plotted as a function of $\mu_0 H_{\perp} / (T - T_C)$. At low magnetic fields, all the curves overlap, confirming the value of T_C determined from transistor measurements. (c) Magnetoconductance as a function of temperature for different fixed magnetic fields $\mu_0 H_{\perp} = 1, 2, 3$, and 4 T. The red dashed line at which magnetoconductance is maximum corresponds to $T_C = 57$ K. The black dashed line marks the transition from positive to negative magnetoconductance ($T = 36$ K). (d) Magnetoconductance traces as a function of magnetic field $\mu_0 H_{\perp}$ for temperatures between $T = 44$ K to $T = 28$ K in 4 K steps. The traces are offset for clarity and the grey dashed line indicates the zero line for each trace, respectively. Red curves correspond to measurements performed with the magnetic field swept from negative to positive values; blue curves correspond to data taken by sweeping the field in the opposite direction.

The tunneling magnetoconductance can then be used to probe the properties of the magnetic state, as shown previously for CrI_3 , CrCl_3 , CrBr_3 , and MnPS_3 multilayers [11, 16, 17, 29, 30, 33, 36, 37]. Distinct features in $\delta G(H_{\perp}, T)$ can be identified near 60 K and 40 K. For T close to 57 K, we observe a positive magnetoconductance exhibiting the same trends observed in our transistor devices, *i.e.*, the manifestation of the critical regime near a ferromagnetic phase transition that originates from the divergence of the magnetic susceptibility at T_C . To confirm this conclusion, Fig. 4a,b show magnetoconductance traces measured at different temperatures and the same data plotted as a function of $\mu_0 H_{\perp} / (T - T_C)$ (using $T_C = 57$ K). All curves collapse again on top of each other for sufficiently small H_{\perp} , therefore, confirming that T_C of thick exfoliated VI_3 multilayers is 57 K (or, again, between 56 K and 58 K, since magnetoconductance traces were measured with a 2 K interval), and not 50 K as in bulk crystals.

Well below T_C , however, the tunneling magnetoconductance exhibits a behavior different from that seen in CrBr_3 barriers. In CrBr_3 barriers, the tunneling

magnetoconductance decreases and becomes vanishingly small at low temperature, but remains always positive [30]. This is a direct consequence of the increase of the spontaneous magnetization of an Ising ferromagnet upon cooling: as the barrier is nearly completely spontaneously magnetized at low temperature, the application of a magnetic field increases the magnetization only slightly and has therefore little influence on the conductance. For VI_3 barriers, instead, when T is lowered below T_C the magnetoconductance vanishes at approximately $T = 36$ K, and becomes negative upon further cooling, as shown in Fig. 4c. The change from positive to negative magnetoconductance is also apparent in Fig. 4d, which shows δG as a function of $\mu_0 H_{\perp}$ for different values of T : indeed, the magnetoconductance increases upon increasing $\mu_0 H_{\perp}$ for $T > 36$ K and decreases upon increasing $\mu_0 H_{\perp}$ for lower temperatures (the data also allow us to determine the coercive field, close to 3 T at $T = 4.2$ K, significantly larger than the value measured in bulk crystals, just above 1 T).

Finally, Fig 5a shows the dependence of the magnetoconductance $\delta G(\mu_0 H_{\parallel}, T)$ with magnetic field $\mu_0 H_{\parallel}$

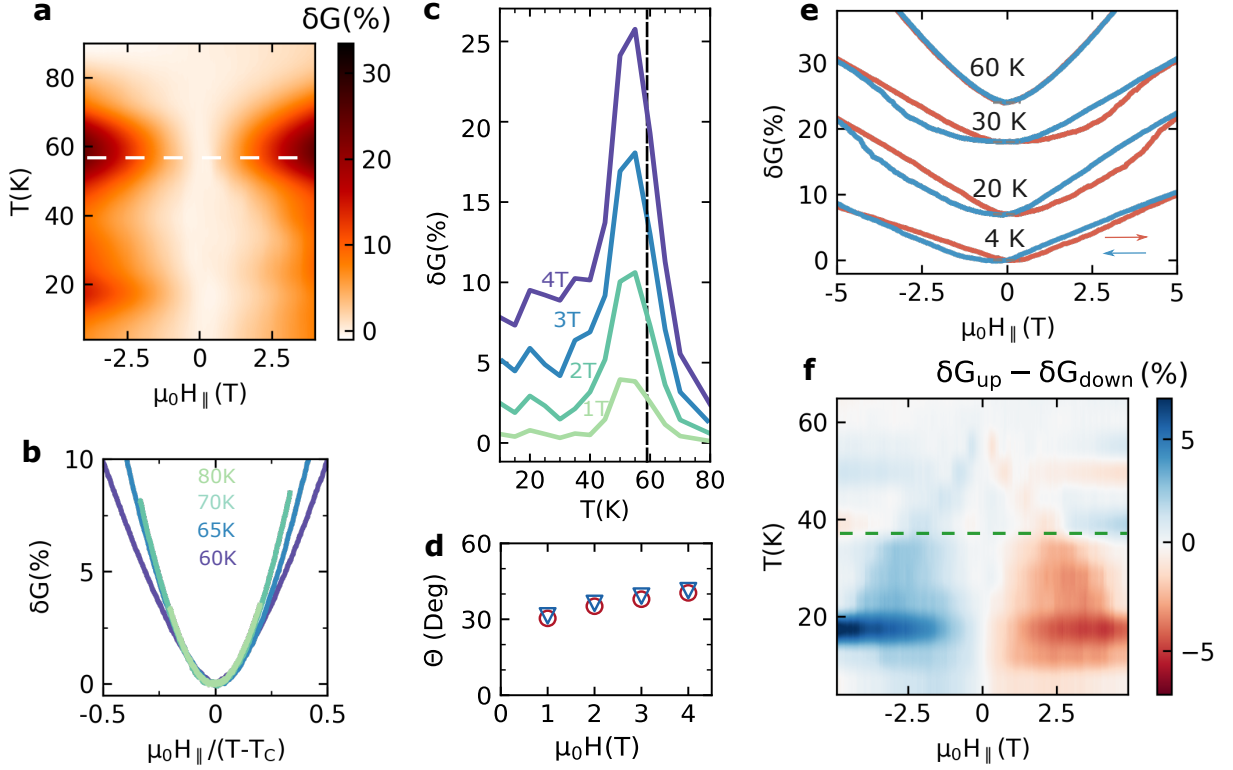


FIG. 5. **(a)** Color plot of the tunneling magnetoconductance δG as a function of temperature T and magnetic field applied parallel $\mu_0 H_{\parallel}$ to the VI_3 planes (data interpolated from magnetoconductance curves measured every 5 K). The two magnetoconductance lobes centered around the Curie temperature (white dashed line indicates $T = 57$ K) also develop in this case. **(b)** Magnetoconductance δG as a function of $\mu_0 H_{\parallel}/(T - T_C)$, measured at temperatures above the ferromagnetic transition (from 60 K to 80 K), showing the collapse of all curves at small applied field. **(c)** Magnetoconductance as a function of temperature $\delta G(T)$ for fixed positive magnetic fields $\mu_0 H_{\parallel}$. The dashed line marks the Curie temperature $T_C = 57$ K. In contrast with the out-plane magnetoconductance, the in-plane magnetoconductance remains always positive down to the lowest temperature investigated. **(d)** Calculated angle of the easy-axis Θ from measured values of $\delta G(H_{\parallel})$ and $\delta G(H_{\perp})$ at $T \sim T_C$ as a function of the applied magnetic field $\mu_0 H$. Blue and red filled circles represent the angle for the 7 nm and 11 nm, respectively. **(e)** $\delta G(\mu_0 H_{\parallel})$ curves for representative temperatures T , ranging from above to well below the Curie temperature (60 K, 30 K, 20 K and 4 K; the traces are offset for clarity). Solid red and blue curves represent the magnetoconductance measured while sweeping the magnetic field $\mu_0 H_{\parallel}$ from negative to positive values or from positive to negative values, respectively. A small hysteresis is present at all temperature below T_C , and it becomes very pronounced for temperatures close to 40 K, as shown in the color plot in **(f)**, which shows the difference between magnetoconductance ($\delta G_{\text{up}} - \delta G_{\text{down}}$) measured while sweeping the field in opposite directions (the green dashed line corresponds to $T = 36$ K, *i.e.*, the temperature at which the magnetoconductance measured as a function of perpendicular field becomes negative, see Fig. 2; the plot shows an interpolation of magnetoconductance traces taken every 5 K).

applied parallel to the VI_3 planes. Even in this case, we observe the characteristic manifestation of the critical regime near the ferromagnetic transition (see the lobes of enhanced magnetoconductance for T close to $T_C = 57$ K in Fig. 5a), and the low-field collapse of the magnetoconductance curves plotted versus $\mu_0 H_{\parallel}/(T - T_C)$ (see Fig. 5b). Correspondingly, $\delta G(\mu_0 H_{\parallel}, T)$ measured at fixed field as a function of T peaks at T_C , reaching values of 25 %, comparable to, but smaller than, the values measured when the field is applied perpendicular to the layers. This difference carries important information because the relative intensity of the magnetoconductance peaks near T_C measured with field applied perpendicular or parallel to the VI_3 layers allows determining the

angle between the easy axis and the normal to the planes.

For a strongly anisotropic easy-axis ferromagnetic tunnel barrier just above T_C (*i.e.*, in the paramagnetic state), the low-field magnetoconductance is proportional to the square of the magnetization, given by the magnetic susceptibility multiplied by the component of the applied field along the easy axis [30]. For the same value of magnetic field applied either in-plane or perpendicular to the plane, the ratio $\delta G(H_{\parallel})/\delta G(H_{\perp})$ is thus given by the square of the ratio of the projections of the magnetic field along the easy axis, and can be used to calculate the angle $\Theta = \tan^{-1}(\sqrt{\delta G(H_{\parallel})/\delta G(H_{\perp})})$ between the easy axis and the direction normal to the VI_3 planes.

The measurements should ideally be performed at small magnetic field (to ensure that the linear relation between M and H holds true), but with a field sufficiently large to have a signal well above the noise. In Figure 5d we show the derived angle for fields between 1 T and 4 T, for two different devices, giving virtually identical results. We see that the angle between the easy axis and the direction normal to the VI_3 layers depends only weakly on field and approaches 30° at 1 T, close to (but slightly smaller than) the one obtained from magnetization measurements performed on as-grown bulk crystals [21].

Upon cooling below T_C the magnetoconductance measured with field applied parallel to the plane decreases monotonously, and remains positive down to $T = 4$ K. However, just under 40 K, a pronounced increase in hysteresis sets in (Fig. 5e-f), which was not reported for CrBr_3 tunnel barriers [30]. We conclude that for temperatures below 40 K magnetotransport measurements indicate a crossover to a regime qualitatively different from that of an established Ising ferromagnet such as CrBr_3 [30]. This crossover is signaled by a change in the sign of the magnetoconductance in perpendicular magnetic field and by a concomitant pronounced increase in the hysteresis of the magnetoconductance measured versus in-plane magnetic field. Such a crossover occurs in the same temperature range in which an anomalous evolution of different magnetic properties takes place in bulk crystals, signaling that the magnetic state of exfoliated layers and bulk crystals are closely related (despite the differences in structural properties, in critical temperature, and coercive field).

The comparison of magnetotransport and magneto-optical experiments allows us to conclude that the observed phenomenology originates from the evolution of the in-plane component of the magnetization of VI_3 . Indeed, tunneling magnetotransport through ferromagnetic barriers probes the alignment of spins in the material, such that configurations of more aligned spins lead to larger tunneling conductance. The negative magnetoconductance observed in a perpendicular magnetic field, therefore, indicates that below 40 K the misalignment of the spins in the VI_3 multilayers increases rather than decreases upon increasing $\mu_0 H_\perp$. Since RMCD measurements (the ones in Ref. [19] and ours, which are only sensitive to the M_z component of the magnetization [38]) find that M_z keeps increasing when lowering T below 40 K and upon applying a perpendicular magnetic field, the increased spin misalignment necessarily originates from the in-plane component of the magnetization.

The simplest scenario that we can envision is that the in-plane component of the magnetization in different VI_3 layers is not pointing in the same direction and that the relative angle between the in-plane component of the magnetization in adjacent layers depends on the applied

perpendicular magnetic field and on temperature. In such a scenario, when T is lowered below T_C , the total spontaneous magnetization is small and is enhanced by the application of a magnetic field, leading to a positive magnetoconductance. However, as the temperature is lowered and the spontaneous magnetization builds up, this effect of the perpendicular magnetic field decreases, and for $T \ll T_C$ its influence on the magnetoconductance becomes negligible (as found in CrBr_3 tunnel barriers [30]). At that point, any misalignment of the in-plane component of the magnetization in different layers may start to dominate magnetotransport. Interestingly, this scenario provides a mechanism that may explain why the critical temperatures of mono and bilayer VI_3 (60 - 61 K) are slightly larger than that of thicker multilayers. Indeed, if the in-plane component of the magnetization in adjacent layers points in different directions, the effect of the intralayer exchange interaction responsible for the value of T_C measured in isolated monolayers would be slightly weakened in multilayers, by the competition with the interlayer exchange interaction (the microscopic mechanism mediating the coupling between perpendicular magnetic field and in-plane component of the magnetization –implicit in the proposed scenario– remains to be determined).

In summary, tunneling magnetoconductance measurements show that, despite having distinct crystallographic structures, exfoliated thin VI_3 crystals exhibit a magnetic state which resembles the one observed in bulk crystals, with the magnetic easy axis canted away from the normal to the VI_3 layers by a large angle. Even though our measurements do not allow the magnetic state to be determined, they show that an Ising ferromagnetic state is not compatible with experimental observations and that deviations originate from the evolution of the in-plane component of the magnetization. These results illustrate the complementarity of magneto-optical and magnetotransport measurements to probe atomically thin 2D magnetic materials, since the commonly employed geometries of RMCD measurements are only sensitive to the component of the magnetization perpendicular to the layers, whereas tunneling magnetoconductance probe phenomena associated to the total magnetization. This conclusion is worth emphasizing because only a few techniques currently have sufficient sensitivity to probe the magnetic properties of atomically thin layers, and it is important to understand which magnetic properties are probed by different measurements.

ACKNOWLEDGEMENTS

The authors gratefully acknowledge Alexandre Ferreira for technical support, Qian Song for help with sample preparation, and Ignacio Gutiérrez-Lezama and Marco Gibertini for fruitful discussions. A. F. Morpurgo gratefully acknowledges the Swiss National

Science Foundation and the EU Graphene Flagship project for support. J. Li, C.A. Occhialini and R. Comin

acknowledge support by the STC Center for Integrated Quantum Materials, NSF Grant No. DMR-1231319.

-
- [1] Novoselov, K. S.; Jiang, D.; Schedin, F.; Booth, T. J.; Khotkevich, V. V.; Morozov, S. V.; Geim, A. K. Two-dimensional atomic crystals. *Proceedings of the National Academy of Sciences* **2005**, *102*, 10451–10453, Publisher: Proceedings of the National Academy of Sciences.
- [2] Mounet, N.; Gibertini, M.; Schwaller, P.; Campi, D.; Merkys, A.; Marrazzo, A.; Sohler, T.; Castelli, I. E.; Cepellotti, A.; Pizzi, G.; Marzari, N. Two-dimensional materials from high-throughput computational exfoliation of experimentally known compounds. *Nature Nanotechnology* **2018**, *13*, 246–252, Number: 3 Publisher: Nature Publishing Group.
- [3] Gong, C.; Li, L.; Li, Z.; Ji, H.; Stern, A.; Xia, Y.; Cao, T.; Bao, W.; Wang, C.; Wang, Y.; Qiu, Z. Q.; Cava, R. J.; Louie, S. G.; Xia, J.; Zhang, X. Discovery of intrinsic ferromagnetism in two-dimensional van der Waals crystals. *Nature* **2017**, *546*, 265–269.
- [4] Huang, B.; Clark, G.; Navarro-Moratalla, E.; Klein, D. R.; Cheng, R.; Seyler, K. L.; Zhong, D.; Schmidgall, E.; McGuire, M. A.; Cobden, D. H.; Yao, W.; Xiao, D.; Jarillo-Herrero, P.; Xu, X. Layer-dependent ferromagnetism in a van der Waals crystal down to the monolayer limit. *Nature* **2017**, *546*, 270–273.
- [5] Burch, K. S.; Mandrus, D.; Park, J.-G. Magnetism in two-dimensional van der Waals materials. *Nature* **2018**, *563*, 47–52.
- [6] Gong, C.; Zhang, X. Two-dimensional magnetic crystals and emergent heterostructure devices. *Science* **2019**, *363*, eaav4450.
- [7] Gibertini, M.; Koperski, M.; Morpurgo, A. F.; Novoselov, K. S. Magnetic 2D materials and heterostructures. *Nature Nanotechnology* **2019**, *14*, 408–419.
- [8] Mak, K. F.; Shan, J.; Ralph, D. C. Probing and controlling magnetic states in 2D layered magnetic materials. *Nature Reviews Physics* **2019**, *1*, 646–661.
- [9] Huang, B.; McGuire, M. A.; May, A. F.; Xiao, D.; Jarillo-Herrero, P.; Xu, X. Emergent phenomena and proximity effects in two-dimensional magnets and heterostructures. *Nature Materials* **2020**, *19*, 1276–1289.
- [10] Sun, Z. et al. Giant nonreciprocal second-harmonic generation from antiferromagnetic bilayer CrI₃. *Nature* **2019**, *572*, 497–501.
- [11] Klein, D. R.; MacNeill, D.; Song, Q.; Larson, D. T.; Fang, S.; Xu, M.; Ribeiro, R. A.; Canfield, P. C.; Kaxiras, E.; Comin, R.; Jarillo-Herrero, P. Enhancement of interlayer exchange in an ultrathin two-dimensional magnet. *Nature Physics* **2019**, *15*, 1255–1260.
- [12] Ubrig, N.; Wang, Z.; Teyssier, J.; Taniguchi, T.; Watanabe, K.; Giannini, E.; Morpurgo, A. F.; Gibertini, M. Low-temperature monoclinic layer stacking in atomically thin CrI₃ crystals. *2D Materials* **2019**, *7*, 015007.
- [13] McCreary, A. et al. Distinct magneto-Raman signatures of spin-flip phase transitions in CrI₃. *Nature Communications* **2020**, *11*, 3879, Number: 1 Publisher: Nature Publishing Group.
- [14] Gibertini, M. Magnetism and stability of all primitive stacking patterns in bilayer chromium trihalides. *Journal of Physics D: Applied Physics* **2020**, *54*, 064002, Publisher: IOP Publishing.
- [15] Dillon, J. F.; Kamimura, H.; Remeika, J. P. Magneto-optical properties of ferromagnetic chromium trihalides. *Journal of Physics and Chemistry of Solids* **1966**, *27*, 1531–1549.
- [16] Wang, Z.; Gutiérrez-Lezama, I.; Ubrig, N.; Kroner, M.; Gibertini, M.; Taniguchi, T.; Watanabe, K.; Imamoğlu, A.; Giannini, E.; Morpurgo, A. F. Very large tunneling magnetoresistance in layered magnetic semiconductor CrI₃. *Nature Communications* **2018**, *9*, 2516.
- [17] Wang, Z.; Gibertini, M.; Dumcenco, D.; Taniguchi, T.; Watanabe, K.; Giannini, E.; Morpurgo, A. F. Determining the phase diagram of atomically thin layered antiferromagnet CrCl₃. *Nature Nanotechnology* **2019**, *14*, 1116–1122.
- [18] Son, S.; Coak, M. J.; Lee, N.; Kim, J.; Kim, T. Y.; Hamidov, H.; Cho, H.; Liu, C.; Jarvis, D. M.; Brown, P. A. C.; Kim, J. H.; Park, C.-H.; Khomskii, D. I.; Saxena, S. S.; Park, J.-G. Bulk properties of the van der Waals hard ferromagnet VI₃. *Physical Review B* **2019**, *99*, 041402.
- [19] Lin, Z.; Huang, B.; Hwangbo, K.; Jiang, Q.; Zhang, Q.; Liu, Z.; Fei, Z.; Lv, H.; Millis, A.; McGuire, M.; Xiao, D.; Chu, J.-H.; Xu, X. Magnetism and Its Structural Coupling Effects in 2D Ising Ferromagnetic Insulator VI₃. *Nano Letters* **2021**, *21*, 9180–9186.
- [20] Doležal, P.; Kratochvílová, M.; Holý, V.; Čermák, P.; Sechovský, V.; Dušek, M.; Míšek, M.; Chakraborty, T.; Noda, Y.; Son, S.; Park, J.-G. Crystal structures and phase transitions of the van der Waals ferromagnet V I₃. *Physical Review Materials* **2019**, *3*, 121401.
- [21] Koriki, A.; Míšek, M.; Pospíšil, J.; Kratochvílová, M.; Carva, K.; Prokleška, J.; Doležal, P.; Kaštil, J.; Son, S.; Park, J.-G.; Sechovský, V. Magnetic anisotropy in the van der Waals ferromagnet V I₃. *Physical Review B* **2021**, *103*, 174401.
- [22] Gati, E.; Inagaki, Y.; Kong, T.; Cava, R. J.; Furukawa, Y.; Canfield, P. C.; Bud'ko, S. L. Multiple ferromagnetic transitions and structural distortion in the van der Waals ferromagnet VI₃ at ambient and finite pressures. *Physical Review B* **2019**, *100*, 094408.
- [23] Kong, T.; Stolze, K.; Timmons, E. I.; Tao, J.; Ni, D.; Guo, S.; Yang, Z.; Prozorov, R.; Cava, R. J. VI₃ — a New Layered Ferromagnetic Semiconductor. *Advanced Materials* **2019**, *31*, 1808074.
- [24] Tian, S.; Zhang, J.-F.; Li, C.; Ying, T.; Li, S.; Zhang, X.; Liu, K.; Lei, H. Ferromagnetic van der Waals Crystal VI₃. *Journal of the American Chemical Society* **2019**, *141*, 5326–5333.
- [25] Valenta, J.; Kratochvílová, M.; Míšek, M.; Carva, K.; Kaštil, J.; Doležal, P.; Opletal, P.; Čermák, P.; Proschek, P.; Uhlířová, K.; Prchal, J.; Coak, M. J.; Son, S.; Park, J.-G.; Sechovský, V. Pressure-induced large increase of Curie temperature of the van der Waals

- ferromagnet V I 3. *Physical Review B* **2021**, *103*, 054424.
- [26] Marchandier, T.; Dubouis, N.; Fauth, F.; Avdeev, M.; Grimaud, A.; Tarascon, J.-M.; Rousse, G. Crystallographic and magnetic structures of the VI 3 and LiVI 3 van der Waals compounds. *Physical Review B* **2021**, *104*, 014105.
- [27] Lyu, B. et al. Probing the Ferromagnetism and Spin Wave Gap in VI3 by Helicity-Resolved Raman Spectroscopy. *Nano Letters* **2020**, *20*, 6024–6031.
- [28] Broadway, D. A.; Scholten, S. C.; Tan, C.; Dontschuk, N.; Lillie, S. E.; Johnson, B. C.; Zheng, G.; Wang, Z.; Oganov, A. R.; Tian, S.; Li, C.; Lei, H.; Wang, L.; Hollenberg, L. C. L.; Tetienne, J. Imaging Domain Reversal in an Ultrathin Van der Waals Ferromagnet. *Advanced Materials* **2020**, *32*, 2003314.
- [29] Kim, H. H. et al. Evolution of interlayer and intralayer magnetism in three atomically thin chromium trihalides. *Proceedings of the National Academy of Sciences* **2019**, *116*, 11131–11136.
- [30] Wang, Z.; Gutiérrez-Lezama, I.; Dumcenco, D.; Ubrig, N.; Taniguchi, T.; Watanabe, K.; Giannini, E.; Gibertini, M.; Morpurgo, A. F. Magnetization dependent tunneling conductance of ferromagnetic barriers. *Nature Communications* **2021**, *12*, 6659.
- [31] Zomer, P. J.; Dash, S. P.; Tombros, N.; van Wees, B. J. A transfer technique for high mobility graphene devices on commercially available hexagonal boron nitride. *Appl. Phys. Lett.* **2011**, *99*, 232104.
- [32] Klein, D. R.; MacNeill, D.; Lado, J. L.; Soriano, D.; Navarro-Moratalla, E.; Watanabe, K.; Taniguchi, T.; Manni, S.; Canfield, P.; Fernández-Rossier, J.; Jarillo-Herrero, P. Probing magnetism in 2D van der Waals crystalline insulators via electron tunneling. *Science* **2018**, eaar3617.
- [33] Song, T.; Cai, X.; Tu, M. W.-Y.; Zhang, X.; Huang, B.; Wilson, N. P.; Seyler, K. L.; Zhu, L.; Taniguchi, T.; Watanabe, K.; McGuire, M. A.; Cobden, D. H.; Xiao, D.; Yao, W.; Xu, X. Giant tunneling magnetoresistance in spin-filter van der Waals heterostructures. *Science* **2018**, eaar4851.
- [34] Kim, H. H.; Yang, B.; Patel, T.; Sfigakis, F.; Li, C.; Tian, S.; Lei, H.; Tsen, A. W. One Million Percent Tunnel Magnetoresistance in a Magnetic van der Waals Heterostructure. *Nano Letters* **2018**, *18*, 4885–4890.
- [35] Fowler, R. H.; Nordheim, L. Electron emission in intense electric fields. *Proceedings of the Royal Society of London. Series A, Containing Papers of a Mathematical and Physical Character* **1928**, *119*, 173–181.
- [36] Long, G.; Henck, H.; Gibertini, M.; Dumcenco, D.; Wang, Z.; Taniguchi, T.; Watanabe, K.; Giannini, E.; Morpurgo, A. F. Persistence of Magnetism in Atomically Thin MnPS3 Crystals. *Nano Letters* **2020**, *20*, 2452–2459.
- [37] Ghazaryan, D. et al. Magnon-assisted tunnelling in van der Waals heterostructures based on CrBr3. *Nature Electronics* **2018**, *1*, 344–349.
- [38] Blundell, S. *Magnetism in Condensed Matter*; OUP Oxford, 2001.